Resource

Cell Reports

# Transcriptional Landscape of Cardiomyocyte Maturation

## Graphical Abstract

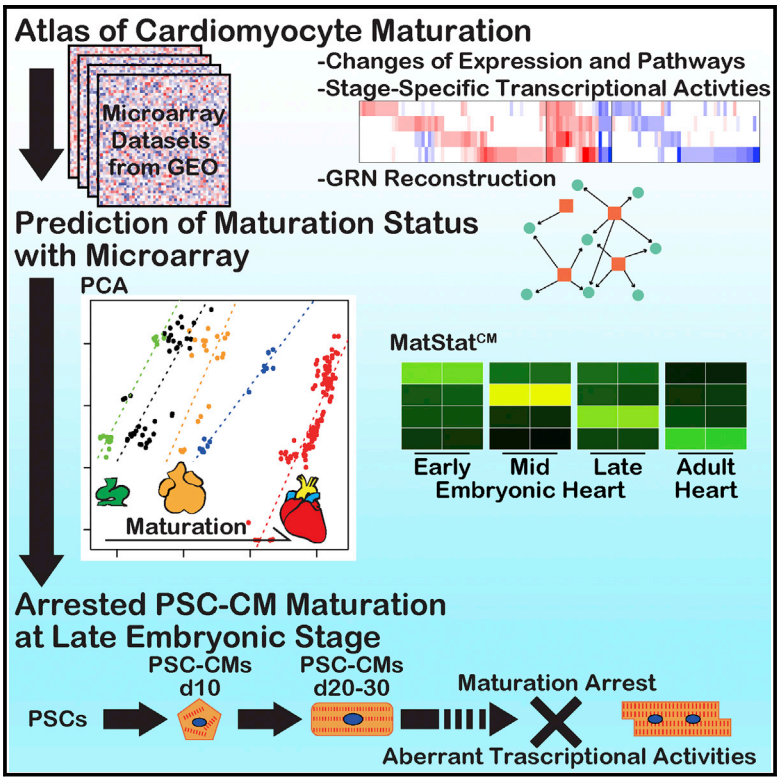


## Authors

Hideki Uosaki, Patrick Cahan, Dong I. Lee, ..., Laviel Fernandez, David A. Kass, Chulan Kwon

## Correspondence

ckwon13@jhmi.edu

## In Brief

Based on maturation stage-specific gene regulatory networks, Uosaki et al. develop a method to assess the maturation status of cardiomyocytes and find that the maturation of PSC-CMs is arrested at a late embryonic stage with inactive PPARs and active CTNNB1.

## Highlights

- Transcriptional landscape during cardiomyocyte maturation
- A GRN-based method to assess maturation status of cardiomyocytes is developed
- PSC-CMs undergo maturation but are arrested at the late embryonic stage
- Misregulated transcriptional factors may alter PSC-CM maturation in vitro

## Accession Numbers

GSE73233

Uosaki et al., 2015, Cell Reports *13*, 1705–1716
November 24, 2015 
http://dx.doi.org/10.1016/j.celrep.2015.10.032

Cell Reports
Resource



# Transcriptional Landscape of Cardiomyocyte Maturation

Hideki Uosaki,[1,2] Patrick Cahan,[3,4,5,6] Dong I. Lee,[1] Songnan Wang,[1,2] Matthew Miyamoto,[1,2] Laviel Fernandez,[1,2] David A. Kass,[1] and Chulan Kwon[1,2,*]
[1]Division of Cardiology, The Johns Hopkins University School of Medicine, Baltimore, MD 21205, USA
[2]The Johns Hopkins Institute for Cell Engineering, Baltimore, MD 21205, USA
[3]Stem Cell Transplantation Program, Division of Pediatric Hematology and Oncology, Manton Center for Orphan Disease Research, Howard Hughes Medical Institute, Boston Children's Hospital and Dana Farber Cancer Institute, Boston, MA 02115, USA
[4]Department of Biological Chemistry and Molecular Pharmacology, Harvard Medical School, Boston, MA 02115, USA
[5]Harvard Stem Cell Institute, Cambridge, MA 02138, USA
[6]Present address: Institute for Cell Engineering and Department of Biomedical Engineering, Johns Hopkins University School of Medicine, Baltimore, MD 21205, USA
*Correspondence: ckwon13@jhmi.edu
http://dx.doi.org/10.1016/j.celrep.2015.10.032


## SUMMARY

**Decades of progress in developmental cardiology has advanced our understanding of the early aspects of heart development, including cardiomyocyte (CM) differentiation. However, control of the CM maturation that is subsequently required to generate adult myocytes remains elusive. Here, we analyzed over 200 microarray datasets from early embryonic to adult hearts and identified a large number of genes whose expression shifts gradually and continuously during maturation. We generated an atlas of integrated gene expression, biological pathways, transcriptional regulators, and gene regulatory networks (GRNs), which show discrete sets of key transcriptional regulators and pathways activated or suppressed during CM maturation. We developed a GRN-based program named MatStat$^{CM}$ that indexes CM maturation status. MatStat$^{CM}$ reveals that pluripotent-stem-cell-derived CMs mature early in culture but are arrested at the late embryonic stage with aberrant regulation of key transcription factors. Our study provides a foundation for understanding CM maturation.**

## INTRODUCTION

The term "development" refers to the process of growing from an immature pluripotent condition to one of organ-/cell-specific maturity. Over the past few decades, major advances have been made in understanding heart development. However, these efforts mostly focused on early developmental processes such as cell differentiation and proliferation (Kathiriya et al., 2015; Kwon et al., 2009; O'Meara et al., 2015; Shenje et al., 2014; Srivastava, 2006), while control over maturation remains largely unknown. This lack of the knowledge may be attributed to the nature of maturation that typically occurs over a long period of time following terminal differentiation.

The maturation of cardiomyocytes (CMs) initiates at mid-gestation and continues until adulthood. During this process, CMs gradually become elongated and rectangular, and the sarcomeres align and organize (Hirschy et al., 2006; Hoshino et al., 2012). To propagate electrical activity into the CMs, transverse tubules (T-tubules) invaginate into the cells during postnatal development (Di Maio et al., 2007; Ziman et al., 2010). Intercalated discs connect CMs to neighboring CMs to allow simultaneous contraction. Connexin 43 and N-cadherin, key components of intercalated discs, are expressed in CMs from early development, but specifically localize to intercalated discs postnatally (Vreeker et al., 2014). These structures are indispensable to CM function. Morphological and structural changes, coupled with gene expression changes, such as isoform switches of sarcomere proteins, occur simultaneously, suggesting common transcriptional regulatory mechanisms may control CM maturation.

Pluripotent stem cells (PSCs) hold great promise for regenerative medicine, disease modeling, and drug discovery because they can differentiate into any cell types in the body with a patient-specific genetic background. Methods to differentiate of PSCs in vitro have been reported (Hayashi et al., 2011; Yamashita et al., 2000). PSC-derived CMs (PSC-CMs) are among the most desired and studied cell types as live CMs are rarely ever obtained from patients. Although PSC-CMs can be efficiently induced from PSCs (Kattman et al., 2011; Uosaki et al., 2011), proper maturation of PSC-CMs remains a critical hurdle for recapitulating the adult phenotype. Recent studies have suggested long-term culture, extrinsic stimuli, or culturing on micropatterned substrates may improve cell morphology and enhance CM maturation (Lundy et al., 2013; Salick et al., 2014; Yanagi et al., 2007; Yang et al., 2014). However, whether these cells truly mature for meaningful use as a model for adult-heart diseases has not been established.

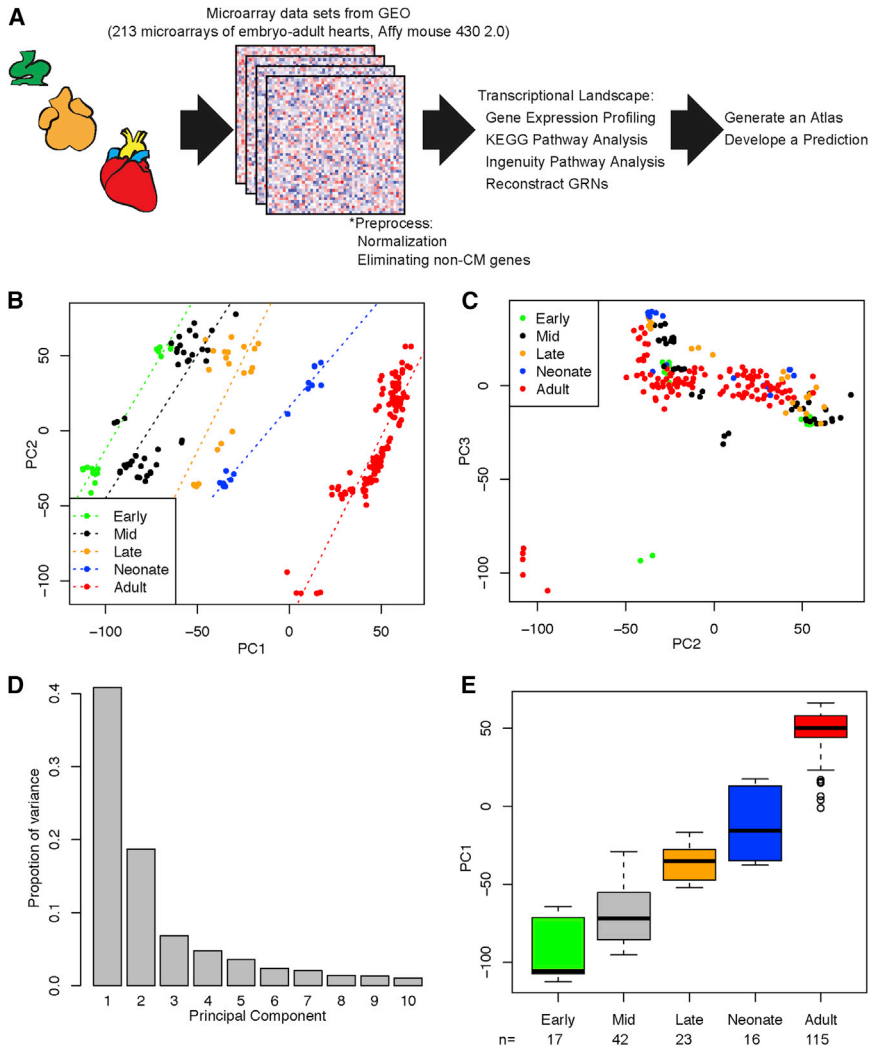


**Figure 1. Principal Component Analysis of CM Maturation**

(A) Experimental scheme. We obtained cardiac microarray datasets from GEO, ranging from early embryonic to adult hearts. Using the datasets, we dictated transcriptional landscape of cardiomyocyte maturation with gene expression profile, biological function (KEGG pathway), upstream transcriptional regulators (using IPA) and reconstructing GRNs. These analyses were integrated to generate an atlas and prediction of cardiomyocyte maturation.

(B and C) PCA plots of 213 microarray datasets. Early embryonic (E8–E11, n = 17, green), mid-embryonic (E12–E14, n = 39, black), late embryonic (E16–E18, n = 26, orange), postnatal (P3–P10, n = 16, blue), and adult (n = 114, red). (B) Plot of PC1 and PC2. Linear regression lines for each stage were shown. Samples were clustered and aligned through PC1 axis as maturation progress. (C) Plot of PC2 and PC3. Most of the samples were clustered and no pattern for maturation was evident.

(D) Proportion of variances in each principal component. PC1 and PC 2 represented ~60% of variance in original data.

(E) Box plot of PC1 value for each stage. Box represents 25$^{th}$ to 75$^{th}$ percentile, mid lines indicate median, and the whiskers show the smallest to largest values. Outliers (more than 2SD) were shown as circles.

See also Figure S1 and Table S1.

## RESULTS

### Global Gene Expression Patterns during Heart Maturation

To assess altered gene expression patterns in developing hearts, we performed a meta-microarray analysis with datasets deposited to Gene Expression Omnibus (GEO). We obtained 39 microarray experiments on the Affymetrix mouse 430 2.0 platform (Table S1) annotated with heart and/or CM, which consist of 658 microarray datasets. Among the 658, 492 microarray datasets were directly related to hearts, CMs, and PSCs differentiated toward CMs. We further narrowed the analysis to 213 microarray datasets of wild-type mouse embryos, neonates, and adults, obtained under normal physiological conditions (Figure 1A). As the heart is composed of CMs and non-CMs such as endothelial cells and fibroblasts, we eliminated genes enriched in non-CMs using purified CM data at mid-embryonic and postnatal stages (Ieda et al., 2009; 2010), which yielded 17,848 genes.

To analyze overall gene expression patterns of the selected data, we used principal component analysis (PCA), which is a standard statistical method to compress and summarize entire microarray information to two or three dimensions, while retaining most of the expression variation in the data (Figures 1B–1D and S1) (Raychaudhuri et al., 2000; Ringnér, 2008). In the PCA plots (Figures 1B and 1C), respective stages were colored. In

Understanding the transcriptional landscape, including gene expression profiles, signaling pathways, and upstream transcriptional regulators, has yielded major insights into development and disease processes (McKinney-Freeman et al., 2012; Miller et al., 2014). For instance, earlier cardiac transcriptome studies revealed a congenital heart disease interactome (Li et al., 2014) or regulation of CM proliferation and heart regeneration (Gan et al., 2015; O'Meara et al., 2015). Recent advances in bioinformatics have allowed reconstruction of gene regulatory networks (GRNs) from expression profiles (Cahan et al., 2014; McKinney-Freeman et al., 2012; Miller et al., 2014). Here, we examined multi-stage microarray datasets obtained from developing hearts and generated an atlas of gene expression, pathways and transcriptional regulators, and reconstructed GRNs during CM maturation. We developed a microarray-based program that can index CM maturation status, named MatStat$^{CM}$. Based on these, we show PSC-CMs undergo maturation early but this becomes arrested at a late embryonic stage even after long-term culture. We further identified transcriptional regulators defective in PSC-CMs that may cause maturation arrest.

the plot of the first principal component (PC1) and PC2, samples from each stage were well aligned (Figure 1B). In contrast, in the plot of PC2 and PC3, most of samples were clustered, and seven outliers were observed (Figure 1C). PC1 accounted for 40.9% of variations of the original data (Figure 1D). PC2 and PC3 accounted for 18.7% and 6.8%, respectively. The rest of PCs accounted for <5% (Figure 1D). Given that PC1 accounted for the major portion of variations, the constant increases in PC1 values from early to late developmental stages (Figures 1B and 1E) suggest that overall gene expression shifts continually in a unidirectional fashion. Samples from each stage were clustered to two in PC2 values; however, they may reflect lab-to-lab variations as samples from a single experiment were clustered to one side (Figures S1A and S1C). One experiment (GEO: GSE1479) used atria and ventricles rather than entire hearts. Notably, both atria and ventricles increased PC1 values at later stages, implying that maturation-related genes might be similarly regulated in both chambers (Figure S1B). While atria had significantly lower values than ventricles, this is likely due to the weights of ventricle-specific genes in calculating PC1 values. These data suggest that overall gene expression patterns change gradually over the course of CM maturation.

## An Atlas of Temporal Gene Expression and Regulation during Heart Maturation

Because PCA revealed gradual and unidirectional transcriptional changes during maturation, we next explored how differentially regulated genes are involved in biological functions and in turn how the transcriptional changes are regulated. To this end, we developed a multilayered atlas of gene expression and regulation, temporal changes of gene expression, pathways, and upstream transcriptional regulators from one stage to the next. First, we selected genes that changed at least 2-fold to the next stage ($p < 0.01$); 578 early to mid-embryonic stage, 306 mid- to late embryonic stage, 431 late embryonic to neonatal stage, and 1,152 neonatal to adult stage genes (Figure 2) were identified (a full gene list is found in Table S2). In agreement with PCA observations of gradual and unidirectional changes, most of the genes continued their expression trends (upregulated or downregulated) throughout the stages, and only small subsets returned to the baseline at later stages (Figures 2E–2H).

Second, to determine how the genes are involved in CM function, we used the Kyoto Encyclopedia of Genes and Genomes (KEGG) pathways enrichment analysis with the genes identified (Figures 2I–2P; Table S3). We found that the peroxisome proliferator-activated receptor (PPAR) pathway (mmu03320) is the only pathway enriched in all comparisons, indicating the activity of the PPAR pathway increases throughout the maturation. The cardiac muscle contraction pathway (mmu04260) and cardiovascular disease pathways, including dilated cardiomyopathy (DCM, mmu05414), hypertrophic cardiomyopathy (HCM, mmu05410), arrhythmogenic right ventricular cardiomyopathy (ARVD, mmu05412), and viral myocarditis (mmu05416), contain structural genes (e.g., sarcomere, desmosome, and sarcoglycan genes) in different compositions. These cardiac pathways were enriched in the upregulated group of genes up to the neonatal stage. However, none of them were enriched in upregulated genes from neonate to adult, suggesting that the activities of those pathways do not change after the neonatal stage. While the fatty acid metabolism pathway (mmu00071), which is essential for the energy supply to adult CMs, was enriched in the upregulated group of genes during embryonic development, carbohydrate metabolism pathways, including glycolysis (mmu00010), pentose phosphate pathway (mmu00030), fructose and mannose metabolism (mmu00051), and galactose metabolisms (mmu00052), were enriched in the group of downregulated genes at the neonate stage. From the mid-embryonic stages, cell-cycle (mmu04110) and its related pathways were constantly enriched in the group of downregulated genes.

Finally, to determine which upstream transcriptional regulators are involved in maturation in temporal manner, we performed upstream regulator analysis with the ingenuity pathway analysis (IPA) software (http://www.ingenuit.com). This program identifies molecular relationships among genes and infers upstream regulators with its curated database from published studies. IPA software calculates an activation *Z* score of a transcriptional regulator based on the fold change and p value of genes under the control of the regulator between two groups. Thus, activation *Z* scores correspond to activity changes between the two groups. To assess temporal transcriptional changes, we used the differentially regulated genes between one stage and the next as described above for IPA upstream regulator analysis. Based on this analysis, we identified upstream transcriptional regulators activated temporally at each stage of CM maturation (Figures 2Q–2S). Most of the regulators changed their activities at one stage or subsequent two stages (Figures 2Q–2S). While only a small subset of genes identified in Figures 2A–2D overlapped, there were transcriptional regulators that incrementally changed their activities (Figure 2S). This suggests that the transcriptional regulators control different genes at each stage.

Our multilayered and temporal atlas of gene expressions, pathways, and upstream transcriptional regulators reveals the process of CM maturation at the transcriptional level.

## Development of MatStat$^{CM}$ to Predict Maturation Status of CMs

A GRN-based method has emerged as a more reliable way for predicting cell and tissue status than clustering (Cahan et al., 2014). Thus, we tested if GRNs can be used to predict the status of CM maturation. To reconstruct stage-specific GRNs of the heart, we first identified genes that were more predominately expressed in each stage, using a single dataset, covering all stages (GEO: GSE51483; Figures S1C and S3A; Table S4) (Li et al., 2014). Then, to identify the upstream regulators and downstream targets of these genes, we examined a reported pan cell-type and tissue GRN (Cahan et al., 2014). While the generic heart GRN included well-known regulators (e.g., *Nkx2-5*, *Gata4*, *Tbx5*, and *Myocd*), stage-specific GRNs included fewer characterized regulators in the heart (Figures 3A–3D). We trained random forest classifiers for each stage with expression distributions estimated from the GSE51483 training dataset. We assessed the performance of the stage-specific classifier by applying it to independent studies of defined stages of heart development. We found that the GRN-based classification accurately determined the stage of origin of the profiles and could

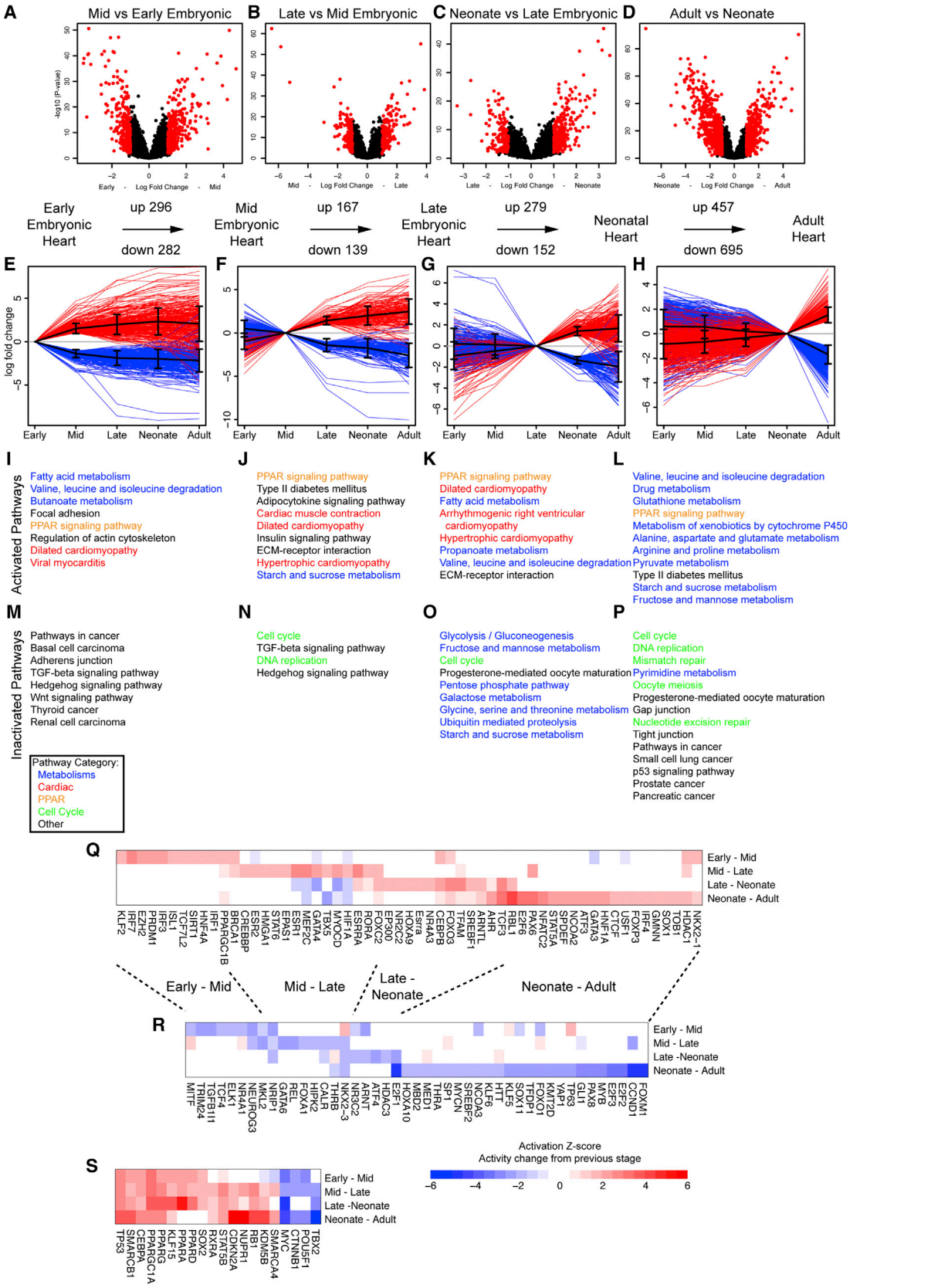


*(legend on next page)*

detect transition of E15.5 and P7 neonatal heart from earlier to later stages (Figures 3E–3H).

## PSC-CMs Matured to Late Embryonic-Neonatal Stage in Culture

We next asked whether PSC-CMs mature into adult-like cells and how mature are they in maturation-enhanced conditions. Current approaches have not addressed this question, and so we tested if global gene expression and/or MatStat$^{CM}$ could determine maturation status of PSC-CMs. To do this, we employed a long-term culture condition, previously shown to enhance CM maturation (Lundy et al., 2013; Yanagi et al., 2007). We differentiated mouse PSCs to CMs and cultured them for up to 30 days. PSC-CMs began to beat at days 7–8 after differentiation, and cells were positive for α-actinin, a sarcomere protein, but did not have clear sarcomere pattern at day 10 (Figure 4A). At days 20 and 30, sarcomeres were well aligned (Figure 4A). As mouse PSCs are typically isolated from embryonic day (E) 3.5 embryos, cultured PSC-CMs at days 10 and 20 are presumed to be at mid-embryonic and postnatal stages, respectively, if maturation is regulated intrinsically and progresses the same as its embryonic counterparts.

To assess the maturation status of PSC-CMs cultured in vitro, we imposed microarray data of PSC-CMs to PCA plot and performed MatStat$^{CM}$ analysis (Figures 4B–4D). With PCA to indicate the global gene expression pattern, PSC-CMs positioned around early to mid-embryonic stages at day 10 and moved to late embryonic stage at day 20 (Figure 4B). Notably, PSC-CMs did not reach to the neonatal stage even at day 30. MatStat$^{CM}$ classified PSC-CMs at day 10 to early embryonic stage and PSC-CMs at days 20–30 were classified to mid- to late-embryonic stages (Figure 4C). PSC-CMs robustly exhibited the early embryonic GRN at day 10 and the late embryonic/neonatal GRN at days 20–30 (Figure 4D). PSC-CMs at days 20–30 also increased the adult GRN. Compared to the sharp transition of the GRNs in vivo, the transition of the GRNs in PSC-CMs was dull, suggesting that their gene expression pattern is not coherent as that of endogenous CMs. All of these data suggest that PSC-CMs mature in long-term culture but then arrest at the late embryonic stage.

To ask if these findings correlate with physiological features, we used $Ca^{2+}$ imaging to compare ventricular and atrial CMs (Figures 4E and 4F). We measured intracellular calcium concentration with Fura-2 dye. We plotted the ratiometry of calcium bound (380 nm) and unbound (340 μm) Fura-2 was plotted (Figure 4E), and time-to-peak-50% and time-to-baseline-50% were used to quantitatively assess velocity of the change in intracellular calcium concentration (Figure 4F). Ventricular CMs displayed slow upstroke and downstroke velocities at E12 (238 ± 21 ms and 1,373 ± 42 ms, respectively). Both velocities increased as maturation progressed (up/down: 54 ± 2/944 ± 48 ms at P0, 44 ± 1 ms/320 ± 8 ms at adult). Atrial CMs displayed greater velocities than ventricular CMs and did not change during embryo development (up/down: 54 ± 5/645 ± 84 ms at E12 and 44 ± 1/613 ± 16 ms at P0). While ventricular CMs displayed no difference in F/F0, which corresponds to the degree of change in intracellular calcium concentration, during embryo development (E12: 17 ± 3 and E18: 20 ± 3), atrial CMs displayed significant increase in F/F0 (E12: 10 ± 1 and E18: 23 ± 3). Upstroke and downstroke velocities of the change in intracellular calcium concentration in PSC-CMs increased after long-term culture (up/down: 167 ± 18/1,125 ± 33 at d10, 105 ± 22/760 ± 48 at d20 and 63 ± 10/666 ± 45 at d30). However, while downstroke velocities at days 20 and 30 were greater than P0 ventricular CMs, upstroke velocities were still slower. $Ca^{2+}$ imaging revealed that PSC-CMs matured to late embryonic/neonate stages, but their physiological features were incoherent.

## Putative Causes of Maturation Arrest In Vitro

PCA, MatStat$^{CM}$, and physiological experiments showed that in-vitro-cultured PSC-CMs become similar to the late embryonic stage CMs but did not progress further. This suggests that genes are regulated differently in PSC-CMs during their maturation in vitro. To identify the genes and regulators, we analyzed genes differentially regulated in PSC-CMs by comparing them to late embryonic and neonatal hearts and adult hearts. For this analysis, we focused on the 1,917 genes that were differentially regulated in vivo during maturation. We found that 679 and 571 genes were differentially regulated in day 20–30 PSC-CMs as compared to late embryonic/neonatal hearts (2-fold difference, $p < 0.01$, Figure S3) and adult hearts (at least 4-fold difference, $p < 0.01$, Figure S3), respectively. Next, we used IPA to identify upstream transcriptional regulators showing distinct activities in PSC-CMs compared to in vivo counterparts. Based on their activity changes, we further classified the regulators into eight types (Figure 5). The first four types consisted of regulators with activities similar to their in vivo counterparts at the late embryonic/neonatal or adult stage (Figure 5, i–iv). The next two types exhibited higher activities than late embryonic/neonatal hearts and lower activities than adult hearts and vice versa

**Figure 2. Atlas of Transcriptional Landscape during CM Maturation**

(A–D) Volcano plots of gene expression changes from one stage to the next. Genes with >2-fold change and moderate p values of <0.01 were colored in red.

(E–H) Time course of changes (log2 fold) of individual genes identified in the volcano plots. Red and blue lines indicate genes with expression increased and decreased one stage to the next, respectively. Black lines indicate mean expression changes. Error bars indicate SDs. (E) Genes changed from early to mid-embryonic hearts. (F) Genes changed from mid to late embryonic hearts. (G) Genes changed from late embryonic to neonatal hearts. (H) Genes changed from neonatal to adult hearts.

(I–P) KEGG pathways enriched in the differentially regulated genes ($p < 0.05$ was considered as enriched). Text color represents the pathway categories. Blue, metabolism; red, cardiac; orange, PPAR; green, cell cycle; black, others. (I–L) Pathways enriched in upregulated genes at the corresponding stages. (M–P) Pathways enriched in downregulated genes at the corresponding stages.

(Q–S) Heatmaps of the activation *Z* scores of upstream transcriptional regulators, correspond to activation changes from one stage to the next. Red, higher in later stage; blue, lower in later stage. (Q) Transiently activated regulators. (R) Transiently inactivated regulators. (S) Incrementally changing regulators.

See also Figure S2 and Tables S2 and S3.

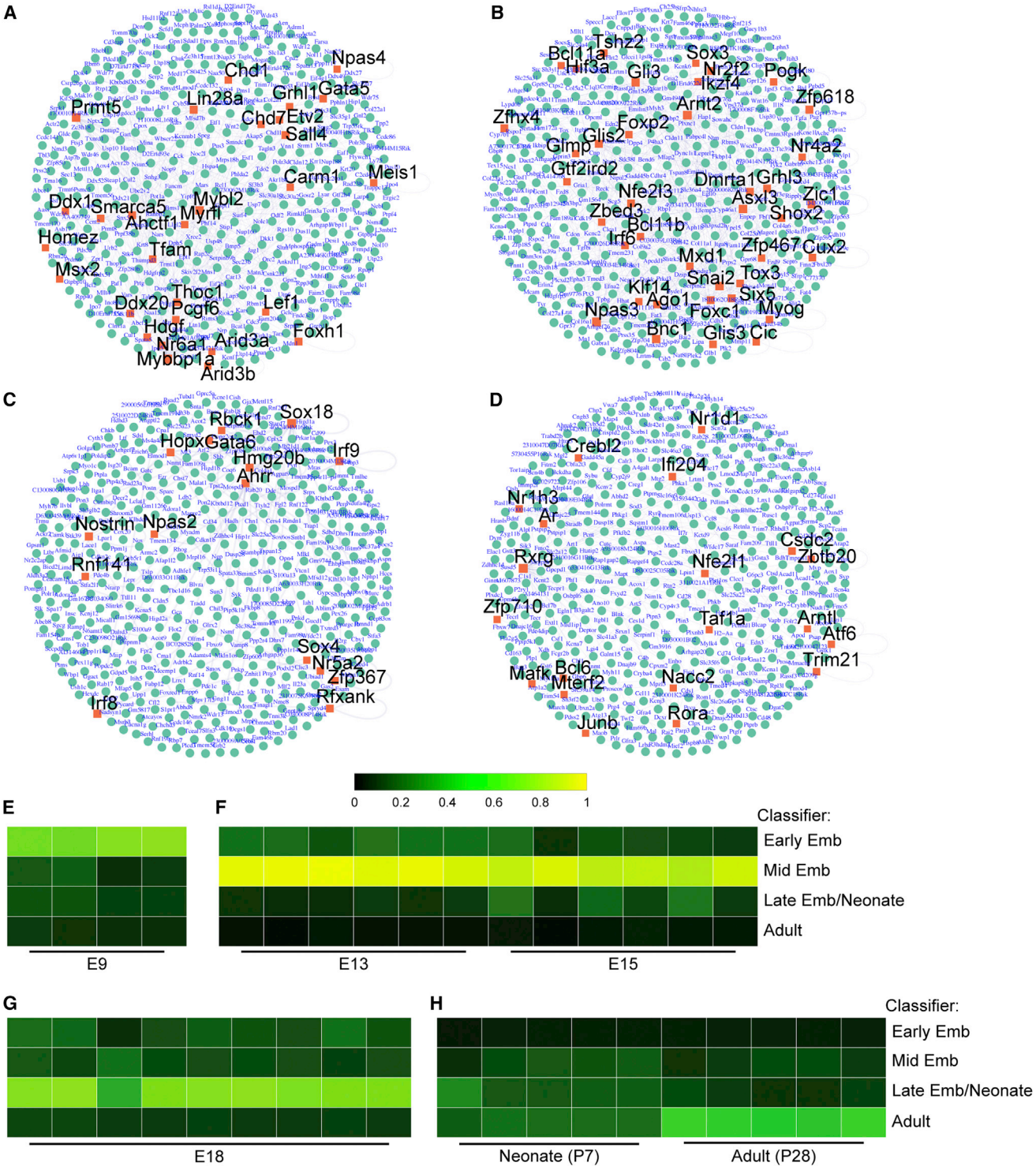


**Figure 3. MatStat$^{CM}$: GRN-Based Prediction System for CM Maturation**

(A–D) Stage-specific GRNs. GRNs of early embryonic (A), mid-embryonic (B), late embryonic/neonatal (C) and adult (D) heart. Each node represents a member of GRN, and factors highlighted in red are transcriptional regulators identified in GRN at each stage. Relationships between regulators and members are shown in lines. All nodes are listed in Table S4.

(E–H) Assessment of performance with independent datasets from E9 (E, GEO: GSE28186), E13-15 (F, GEO: GSE32078), E18 (G, GEO: GSE8199), and P7-adult (H, GEO: GSE38754). Each column represents one microarray dataset and classified values of GRN status for each stage were shown as heatmap.

See also Figure S3 and Table S4.

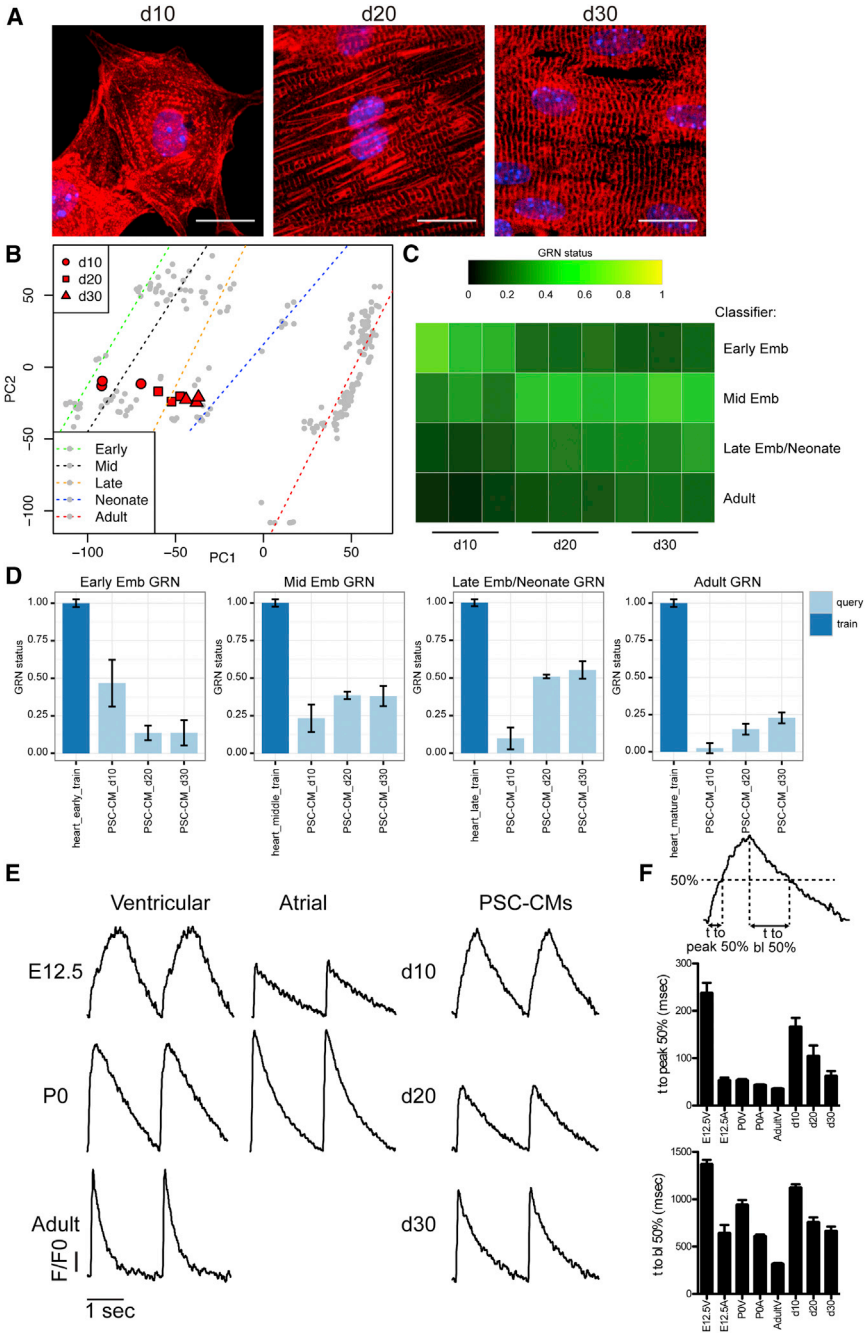


**Figure 4. Maturation of PSC-CMs after Long-Term Culture**

(A) Immunostaining of PSC-CMs with α-actinin at days 10–30. Scale bar, 20 μm.

(B) PCA of 213 microarray, superimposed with PSC-CMs at days 10–30.

(C) MatStat$^{CM}$ analysis. GRN status of PSC-CMs was similar to early embryonic hearts at day 10, and became mid to late embryonic heart at days 20–30.

(D) GRN statuses of PSC-CMs were assessed using the GRN classifiers of each maturation stage. Means + SD are shown (n = 3).

(E) $Ca^{2+}$ transient of embryonic (E12), neonatal, adult CMs and PSC-CMs. Cells were stimulated every 2 s.

(F) Statistics of time (t) to peak 50% and time (t) to baseline (bl) 50% of $Ca^{2+}$ transient. Mean + SEM ($n \geq 9$).

Codes for imposing PSC-CM data to PCA and analyzing with MatStat$^{CM}$ can be found in Data S1.

(Figure 5, v and vi). While they were different from their in vivo counterparts in activity levels, most of their activities shifted into the right direction: the regulators in the classes were activated (Figure 5, v) or inactivated (Figure 5, vi) from neonate to adult (Figure 2). As such, these six types of regulators may not alter the normal trajectory of maturation in vitro. In contrast, the last two types were the groups of regulators whose transcriptional activities were continuously higher or lower than their in vivo counterparts throughout the stages (Figure 5, vii and viii). In particular, regulators incrementally activated throughout the maturation (Figure 2S) were found inactive in PSC-CMs (Figure 5, viii, PPARA/G, PPARGC1A, and CEBPA/B). Similarly, CTNNB1 was incrementally inactivated during maturation in vivo, but remained active in PSC-CMs (Figure 5, vii). Thus, misregulation of these regulators may be responsible for the aberrant maturation of PSC-CMs in vitro.

## DISCUSSION

In the current study, we (1) developed an atlas of temporal gene expression, pathways, and regulations during heart maturation, and (2) established a method to determine CM maturation status with microarray and stage-specific GRNs, named MatStat$^{CM}$ (Figure 6). With the integrated approach, we demonstrated that PSC-CMs can undergo maturation early but arrest at the late embryonic stage after long-term culture. We believe this information will lay the foundation for understanding CM maturation and be instrumental for generating adult CMs from PSCs.

This multilayered analysis provides fascinating insights into understanding CM maturation, which were not demonstrated in previous studies (Li et al., 2014; Gan et al., 2015; O'Meara et al., 2015). We found that the atlas of temporal transcriptional regulations was well correlated with transcriptional and KEGG pathway changes (Figure 2; Tables S2 and S3). Most of the regulators were activated or inactivated only once during maturation (Figure 2Q). According to the IPA results, once a regulator was activated, it remained constantly activated unless inactivated at later stages (Figure 6A). MEF2C, GATA4, TBX5, MYOCD,

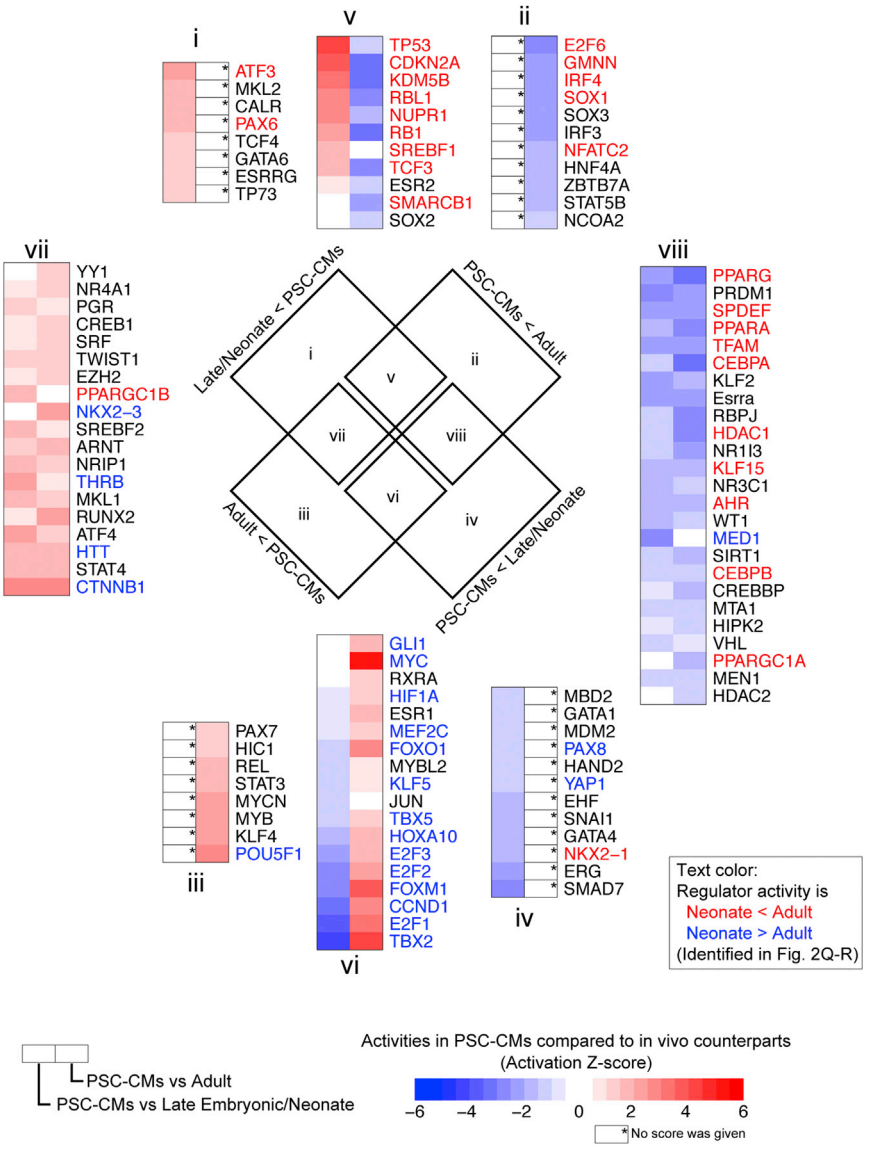


**Figure 5. Comparison of Regulator Activities**

Heatmaps showing transcriptional regulator activities in PSC-CMs compared to late/neonatal (left) and adult (right) hearts. Text color represents activity changes between neonatal and adult stages. Red, activated; blue, inactivated. Identified regulators were classified to eight. Venn diagram of classification is shown in the middle. (i–iv) Transcriptional regulators had activities in PSC-CMs similar to either late embryonic/neonatal or adult hearts: (i) similar to adult and higher than late embryonic/neonatal, (ii) similar to late embryonic/neonatal and lower than adult, (iii) similar to late embryonic/neonatal and higher than adult, and (iv) similar to adult and lower than late embryonic/neonatal. (v and vi) Transcriptional regulators had activities in between the in vivo counterparts: the regulators were activated (v), and inactivated (vi) from late embryonic/neonate to adult. (vii and viii) Misregulated transcriptional regulators in vitro. (vii) Transcriptional regulators had higher activities in PSC-CMs compared to late embryonic/neonatal and adult heart, and (viii) transcriptional regulators had lower activities in PSC-CMs compared to late embryonic/neonatal and adult heart.

See also Figure S4.

and HIF1A were transiently activated factors from mid- to late embryos, Among those genes, MEF2C, GATA4, and TBX5 were known as the essential regulators to convert fibroblasts into CMs in mice, and MYOCD was one of the additional factors necessary for the conversion in human. These findings suggest they play important roles in activating cardiac pathways (Ieda et al., 2010; Wada et al., 2013). However, the cardiac pathways were also enriched in other stages, suggesting the presence of alternative regulators (e.g., Regulators in generic GRNs such as *Hopx* and *Nkx2-5* in the earlier stage, Figure S3). In addition to the activated regulators, there were inactivated regulators. For example, Aryl hydrocarbon receptor nuclear translocator (ARNT) was inactivated at the neonatal stage, suggesting that the regulator may affect its downstream target genes in embryonic hearts. Activation of TP53 and inactivation of MYC cause cell-cycle arrest and are consistent with the pathway analysis that revealed the cell-cycle pathways enriched in downregulated genes during the maturation (Figures 2N–2P; Table S3). They changed their activities incrementally, and additional cell-cycle repressors, retinoblastoma 1 (RB1), retinoblastoma-like 1 (RBL1), and cyclin-dependent kinase inhibitor 2A (CDKN2A) were highly activated, whereas the cell-cycle accelerators, cyclin D1 (CCND1) and E2F1-3 were inactivated in adult. As a result, the cell-cycle pathway was enriched in downregulated genes from the earlier stages, and more cell-cycle-related pathways were enriched in downregulated genes at the adult stage. Interestingly, the PPAR pathway was the only pathway enriched in upregulated genes throughout the maturation. PPAR is considered as a master regulator of fatty acid metabolisms (Evans et al., 2004) and it was incrementally activated through maturation. Pathway analysis also revealed how metabolic changes are accomplished in vivo. Embryonic CMs use glycolysis to generate energy, but adult CMs use fatty acid oxidation (Lopaschuk et al., 1992). During embryonic development, fatty acid metabolism pathway was increased, and glycolysis pathway was decreased upon birth, suggesting that late embryonic CMs could utilize fatty acid but still they use glycolysis due to the limited supply of oxygen.

Previous studies reported enhanced PSC-CM maturation in long-term culture; however, the degree of maturation was unknown. Our approach with a reference from in vivo maturation provided a quantitative perspective on CM maturation, revealing

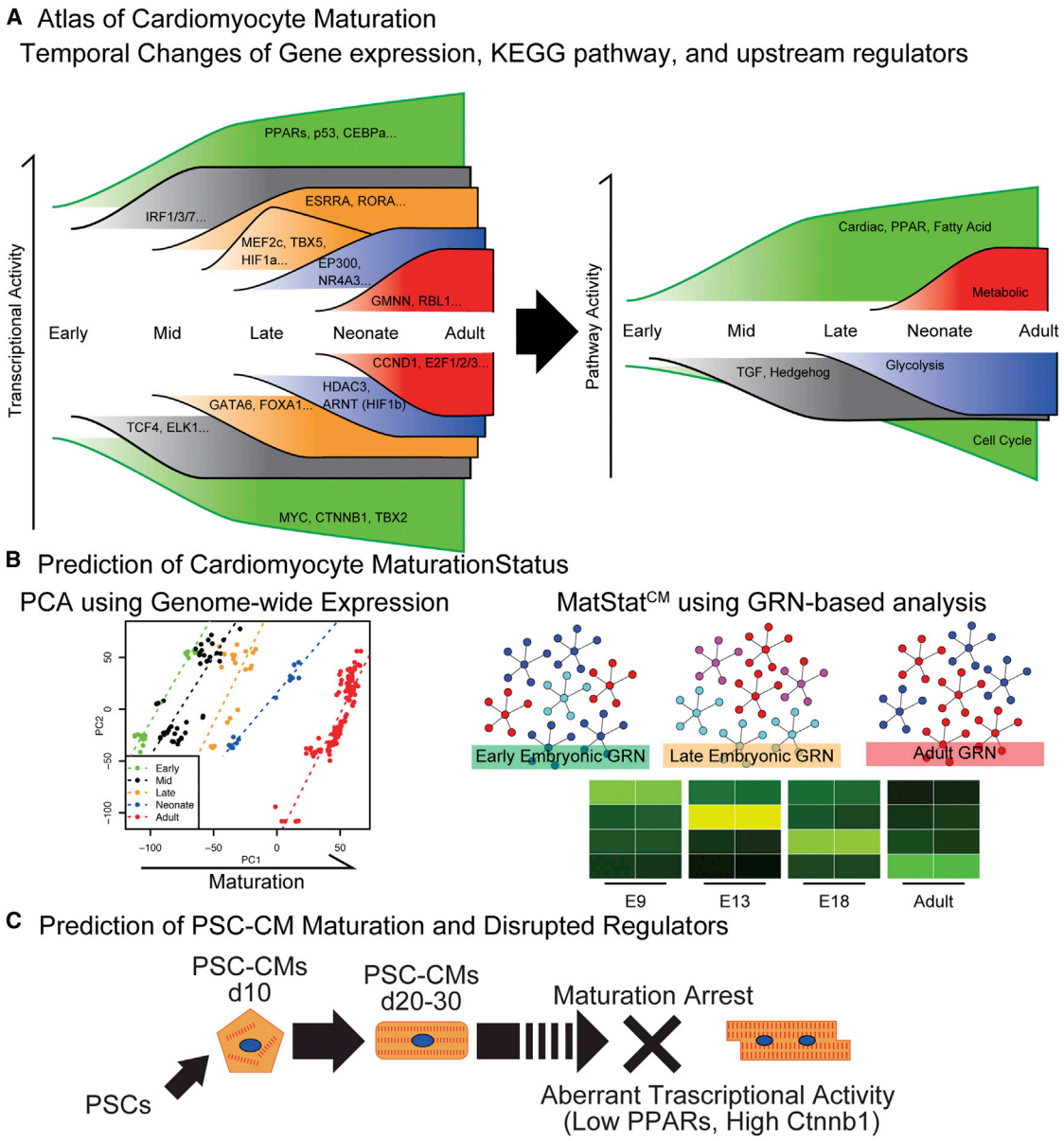


**Figure 6. Summary of the Study**

(A and B) Using microarray analysis, we developed an atlas (A) and a prediction method of CM maturation (B). (A) An atlas of CM maturation showing temporal transcriptional activity and pathway activity changes. (B) Prediction of CM maturation with a GRN-based method, named MatStat$^{CM}$.

(C) We found that PSC-CMs undergo maturation but are arrested at late embryonic to neonatal stage. There were two groups of transcriptional regulators: (1) the activities of transcriptional regulators were between late embryo/neonate and adult, and (2) too high or too low, compared to the in vivo counterpart.

that PSC-CMs progress through maturation but then are unexpectedly arrested at the late embryonic stage after 20 days of culture (Figures 4, 6B, and 6C). Although the global gene expression pattern was close to late embryonic or neonatal hearts, the transition of GRNs was more diffused, and approximately one-third of the genes differentially regulated during maturation were misregulated in PSC-CMs. This implies that the activities of upstream regulators were incoherent in PSC-CMs. Indeed, approximately half of the upstream transcriptional regulators displayed their activities between late embryonic/neonatal and adult or close to either one, suggesting that they are unlikely to cause the arrest. The other half were aberrantly active or inactive as compared to in vivo counterparts, suggesting that they may be responsible for the abnormal maturation. The aberrant regulators include PPARs, PPAR gamma coactivator 1A (PPARGC1A), CCAAT/enhancer binding protein A/B (CEBPA/B), and beta-catenin (CTNNB1). It is intriguing to find them active or inactive because all of them have been implicated in CM

maturation: (1) PPARs regulate fatty acid metabolism in heart and CM-specific deletion of PPARs results cardiac diseases such as cardiomyopathy and hypertrophy (Ahmadian et al., 2013; Finck, 2007), (2) PPARGC1A/B, coactivators of PPARs, and other nuclear receptors, regulate mitochondrial biogenesis in heart (Lehman et al., 2000), (3) CEBPB inhibits CM proliferation and hypertrophy (Boström et al., 2010), (4) activation of CTNNB1 increases CM proliferation and causes sarcomere disarray, suggesting that CTNNB1 alters CM maturation (Tseng et al., 2006; Uosaki et al., 2013), and (5) to recapitulate ARVD, an adult-onset heart disease with pathogenic fatty acid infiltration in CMs and CM loss, with patient-derived hPSC-CMs, a cocktail of chemicals including dexamethasone (NR3C1/glucocorticoid receptor) and Rosiglitazone (PPARD), was used to create a lipogenic condition (Kim et al., 2013). Further studies will be necessary to determine their roles for PSC-CM maturation.

Our method can be applied to the other culture conditions known to enhance CM maturation: long-term culture, supplementation of factors (e.g., thyroid hormone), micro-patterning, and electrical and mechanical stimulation were reported to enhance CM maturation (Chan et al., 2013; Nunes et al., 2013; Salick et al., 2014; Yang et al., 2014). As no tool has been available for maturation analysis, it was almost impossible to compare and determine which maturation method is better and how mature the CMs are in each study. MatStat$^{CM}$ can be a powerful tool to compare and determine CM maturation status, as it is a computer program designed to inform the transcriptional status of CM maturation in a non-biased fashion, developed based on well-standardized microarray platform, and running on statistical software R (Figure 3; see Data S1 for codes and datasets). The limitation of MatStat$^{CM}$ is that the current version only supports the mouse 430 2.0 microarray chip due to the limited number and time points of microarray datasets conducted with other chips, such as newer mouse gene 1.0 ST, chips for human genes and RNA sequencing (RNA-seq). We expect to update/upgrade the prediction program as more information becomes available.

The current study utilized bioinformatics to determine transcriptional networks and regulators during CM maturation. Thus, it will be important to investigate expression kinetics of each transcriptional regulator and its target genes by biochemical methods, such as chromatin immunoprecipitation. Similar to transcriptional regulators, microRNAs (miRNAs) also regulate a large number of genes with specific biological functions (He and Hannon, 2004) and were implicated in CM maturation. For instance, conditional knockout of Dicer1, a key regulator of miRNA biogenesis, in the embryonic heart resulted in dilated cardiomyopathy-like phenotypes with misexpression of cardiac contractile proteins and profound sarcomere disarray, suggesting that miRNAs are involved in maintaining CMs (Chen et al., 2008; da Costa Martins et al., 2008). Given that several miRNAs are involved in CM proliferation and maturation (Cao et al., 2013; Eulalio et al., 2012; Kuppusamy et al., 2015), it will be interesting to study if the transcriptional regulators identified in this research affect maturation-related miRNAs. It would also be important to investigate the role of miRNAs during CM maturation.

## EXPERIMENTAL PROCEDURES

### Microarray Analysis

Microarray analysis used the statistical software Bioconductor R (Gentleman et al., 2004; Huber et al., 2015). We obtained 658 datasets annotated with heart and/or CMs from GEO. List of datasets and a brief description are found in Table S1. We performed frozen robust multi-array average (fRMA) (McCall et al., 2010) to normalized the datasets. To convert probe sets to each gene, we selected a probe-set with widest dynamic range (Seita et al., 2012). We eliminated non-CM-enriched genes in heart (1.5-fold and moderated p value <0.05: ~3,000 genes) (Ieda et al., 2009, 2010). Principal component analysis (PCA) was performed using R function prcomp with standard condition. We used empirical Bayes (limma package) to compare expressions among samples (Ritchie et al., 2015), and thresholds for fold change and moderated p value were determined in the main text and figure legends. Heatmaps were generated using the R function pheatmap. For Kyoto Encyclopedia of Genes and Genomes (KEGG) pathway analysis, we use DAVID Bioinformatics Database (Huang et al., 2009b; 2009a). To infer upstream regulators, we used ingenuity pathway analysis (IPA) (http://www.ingenuit.com). To reconstruct stage-specific GRNs of the heart and assess GRN status, we used pan cell-type and tissue GRNs and the calculation method that has been described and validated (Cahan et al., 2014). Source codes and datasets for PCA, GRN reconstruction, and MatStat$^{CM}$ can be found in Data S1. Codes for CellNet, which are required for GRN reconstruction and MatStat$^{CM}$, are available through github (https://github.com/pcahan1/CellNet).

### PSC Culture and Cardiac Differentiation

Mouse PSCs with a cardiac-specific Ncx1 promoter-driven puromycin resistance gene (Yamanaka et al., 2008) were maintained in 2i medium (Glasgow minimum essential medium with 10% fetal bovine serum, 1,000 U/ml ESGRO [Millipore], 3 μM CHIR99021, 1 μM PD0325901, Glutamax, sodium pyruvate, and MEM non-essential amino acids) (Uosaki et al., 2012). For cardiac differentiation, cells were suspended in serum-free differentiation medium (SFD) (Iscove's modified Dulbecco's medium and F-2 medium, supplemented with B27, N2, Glutamax, ascorbic acid, and 1-thyolglycerol) (Kattman et al., 2011) for 2 days. Cells were subsequently treated with Activin A, bone morphogenetic protein 4 (BMP4), and vascular endothelial growth factor (VEGF) for 2 days. Then, cell clusters were dissociated and replated with basic fibroblast growth factor (bFGF), FGF10, and VEGF for 3 more days. By day 7 after differentiation, cells start self-beating. To eliminate non-cardiac cells, we added puromycin for 2–3 days. At days 9–10, we analyzed CM purity by cardiac troponin T staining (Uosaki et al., 2011) and cells with at least 90% purity were used for further analysis. For long-term culture, we replated differentiated cells at day 9 and cultured up to 30 days after differentiation in SFD medium.

### Immunostaining

For immunostaining, cells were cultured in chamber slide, fixed with 4% paraformaldehyde for overnight, washed with PBS, permeabilized with PBS-Triton X, blocked with 3% BSA in PBS, and incubated with anti-α-actinin antibody (1:500, Sigma-Aldrich) for overnight. Cells were washed and stained with secondary antibody, anti-mouse IgG (1:500, Invitrogen) conjugated with Alexa-Fluor dye (Invitrogen). DNA was stained with DAPI. Images were taken with a confocal microscope (Leica TCS SPE RGBV).

### RNA Purification and Microarray

RNA was isolated from cells using TRIzol following manufacturer instruction and then submitted to microarray core at Johns Hopkins University. The accession number for the full dataset of PSC-CMs reported in this paper is GEO: GSE73233.

### $Ca^{2+}$ Transient

To analyze $Ca^{2+}$ transient with embryonic and postnatal CMs, hearts were minced and enzymatically dissociated with collagenase and trypsin. Cells were then seeded on gelatin or laminin-coated cover glasses in SFD medium supplemented with 10% serum and analyzed the following day. Adult CMs were isolated with Langendorff perfusion and used in the same day (Seo et al., 2014). All mouse procedures were reviewed and approved by the Johns

Hopkins University. PSC-CMs were differentiated as described above and then replated at day 9 for the experiments at day 10 or replated around day 15 for the experiments at day 20 and 30. To assess cytosolic $Ca^{2+}$, cells were loaded with Fura-2 dye in Tyrode's solution for 20 min. Cytosolic $Ca^{2+}$ was monitored with IonOptix system, using excitation wavelengths of 340 and 380 nm to detect Fura-2 fluorescence at 510 nm. Cells were stimulated every 2 s.

## ACCESSION NUMBERS

The accession number for the full dataset of PSC-CMs reported in this paper is GEO: GSE73233.

## SUPPLEMENTAL INFORMATION

Supplemental Information includes four figures, four tables, and one data file and can be found with this article online at http://dx.doi.org/10.1016/j.celrep.2015.10.032.

## AUTHOR CONTRIBUTIONS

Conceptualization, H.U. and C.K.; Methodology, Software, and Formal Analysis, H.U. and P.C.; Investigation, H.U., D.I.L., M.M., S.W., and L.F.; Writing – Original Draft, H.U. and C.K.; Writing – Review & Editing, H.U., D.A.K., and C.K.; Supervision, D.A.K.; Funding Acquisition, H.U. and C.K.

## ACKNOWLEDGMENTS

The authors thank D.A.K. and C.K. laboratory members for helpful discussions and G. Howard for editorial assistance. This work was supported by the Magic that Matters Fund and grants from NHLBI/NIH (R01HL111198) and MSCRF (MSCRFI-1622) to C.K. H.U. was supported by the Japan Heart Foundation/Bayer Yakuhin Research Grant Abroad and fellowships from the Japan Society for the Promotion of Science and MSCRF. P.C. was supported by NIDDK/NIH (K01DK096013). D.A.K. was supported by National Health Service-NHLBI grants HL-119012, HL-107153, and Fondation Leducq.

Received: June 28, 2015
Revised: August 19, 2015
Accepted: October 9, 2015
Published: November 12, 2015

## REFERENCES

Ahmadian, M., Suh, J.M., Hah, N., Liddle, C., Atkins, A.R., Downes, M., and Evans, R.M. (2013). PPARγ signaling and metabolism: the good, the bad and the future. Nat. Med. *19*, 557–566.

Boström, P., Mann, N., Wu, J., Quintero, P.A., Plovie, E.R., Panáková, D., Gupta, R.K., Xiao, C., MacRae, C.A., Rosenzweig, A., and Spiegelman, B.M. (2010). C/EBPβ controls exercise-induced cardiac growth and protects against pathological cardiac remodeling. Cell *143*, 1072–1083.

Cahan, P., Li, H., Morris, S.A., Lummertz da Rocha, E., Daley, G.Q., and Collins, J.J. (2014). CellNet: network biology applied to stem cell engineering. Cell *158*, 903–915.

Cao, X., Wang, J., Wang, Z., Du, J., Yuan, X., Huang, W., Meng, J., Gu, H., Nie, Y., Ji, B., et al. (2013). MicroRNA profiling during rat ventricular maturation: A role for miR-29a in regulating cardiomyocyte cell cycle re-entry. FEBS Lett. *587*, 1548–1555.

Chan, Y.-C., Ting, S., Lee, Y.-K., Ng, K.-M., Zhang, J., Chen, Z., Siu, C.W., Oh, S.K.W., and Tse, H.-F. (2013). Electrical stimulation promotes maturation of cardiomyocytes derived from human embryonic stem cells. J. Cardiovasc. Transl. Res. *6*, 989–999.

Chen, J.-F., Murchison, E.P., Tang, R., Callis, T.E., Tatsuguchi, M., Deng, Z., Rojas, M., Hammond, S.M., Schneider, M.D., Selzman, C.H., et al. (2008). Targeted deletion of Dicer in the heart leads to dilated cardiomyopathy and heart failure. Proc. Natl. Acad. Sci. USA *105*, 2111–2116.

da Costa Martins, P.A., Bourajjaj, M., Gladka, M., Kortland, M., van Oort, R.J., Pinto, Y.M., Molkentin, J.D., and De Windt, L.J. (2008). Conditional dicer gene deletion in the postnatal myocardium provokes spontaneous cardiac remodeling. Circulation *118*, 1567–1576.

Di Maio, A., Karko, K., Snopko, R.M., Mejía-Alvarez, R., and Franzini-Armstrong, C. (2007). T-tubule formation in cardiacmyocytes: two possible mechanisms? J. Muscle Res. Cell Motil. *28*, 231–241.

Eulalio, A., Mano, M., Dal Ferro, M., Zentilin, L., Sinagra, G., Zacchigna, S., and Giacca, M. (2012). Functional screening identifies miRNAs inducing cardiac regeneration. Nature *492*, 376–381.

Evans, R.M., Barish, G.D., and Wang, Y.-X. (2004). PPARs and the complex journey to obesity. Nat. Med. *10*, 355–361.

Finck, B.N. (2007). The PPAR regulatory system in cardiac physiology and disease. Cardiovasc. Res. *73*, 269–277.

Gan, J., Sonntag, H.-J., Tang, M.K., Cai, D., and Lee, K.K.H. (2015). Integrative Analysis of the Developing Postnatal Mouse Heart Transcriptome. PLoS ONE *10*, e0133288.

Gentleman, R.C., Carey, V.J., Bates, D.M., Bolstad, B., Dettling, M., Dudoit, S., Ellis, B., Gautier, L., Ge, Y., Gentry, J., et al. (2004). Bioconductor: open software development for computational biology and bioinformatics. Genome Biol. *5*, R80.

Hayashi, K., Ohta, H., Kurimoto, K., Aramaki, S., and Saitou, M. (2011). Reconstitution of the mouse germ cell specification pathway in culture by pluripotent stem cells. Cell *146*, 519–532.

He, L., and Hannon, G.J. (2004). MicroRNAs: small RNAs with a big role in gene regulation. Nat. Rev. Genet. *5*, 522–531.

Hirschy, A., Schatzmann, F., Ehler, E., and Perriard, J.-C. (2006). Establishment of cardiac cytoarchitecture in the developing mouse heart. Dev. Biol. *289*, 430–441.

Hoshino, S., Omatsu-Kanbe, M., Nakagawa, M., and Matsuura, H. (2012). Postnatal developmental decline in IK1 in mouse ventricular myocytes isolated by the Langendorff perfusion method: comparison with the chunk method. Pflugers Arch. *463*, 649–668.

Huang, W., Sherman, B.T., and Lempicki, R.A. (2009a). Systematic and integrative analysis of large gene lists using DAVID bioinformatics resources. Nat. Protoc. *4*, 44–57.

Huang, W., Sherman, B.T., and Lempicki, R.A. (2009b). Bioinformatics enrichment tools: paths toward the comprehensive functional analysis of large gene lists. Nucleic Acids Res. *37*, 1–13.

Huber, W., Carey, V.J., Gentleman, R., Anders, S., Carlson, M., Carvalho, B.S., Bravo, H.C., Davis, S., Gatto, L., Girke, T., et al. (2015). Orchestrating high-throughput genomic analysis with Bioconductor. Nat. Methods *12*, 115–121.

Ieda, M., Tsuchihashi, T., Ivey, K.N., Ross, R.S., Hong, T.T., Shaw, R.M., and Srivastava, D. (2009). Cardiac fibroblasts regulate myocardial proliferation through beta1 integrin signaling. Dev. Cell *16*, 233–244.

Ieda, M., Fu, J.D., Delgado-Olguin, P., Vedantham, V., Hayashi, Y., Bruneau, B.G., and Srivastava, D. (2010). Direct reprogramming of fibroblasts into functional cardiomyocytes by defined factors. Cell *142*, 375–386.

Kathiriya, I.S., Nora, E.P., and Bruneau, B.G. (2015). Investigating the transcriptional control of cardiovascular development. Circ. Res. *116*, 700–714.

Kattman, S.J., Witty, A.D., Gagliardi, M., Dubois, N.C., Niapour, M., Hotta, A., Ellis, J., and Keller, G. (2011). Stage-specific optimization of activin/nodal and BMP signaling promotes cardiac differentiation of mouse and human pluripotent stem cell lines. Cell Stem Cell *8*, 228–240.

Kim, C., Wong, J., Wen, J., Wang, S., Wang, C., Spiering, S., Kan, N.G., Forcales, S., Puri, P.L., Leone, T.C., et al. (2013). Studying arrhythmogenic right ventricular dysplasia with patient-specific iPSCs. Nature *494*, 105–110.

Kuppusamy, K.T., Jones, D.C., Sperber, H., Madan, A., Fischer, K.A., Rodriguez, M.L., Pabon, L., Zhu, W.-Z., Tulloch, N.L., Yang, X., et al. (2015). Let-7 family of microRNA is required for maturation and adult-like metabolism in

stem cell-derived cardiomyocytes. Proc. Natl. Acad. Sci. USA *112*, E2785–E2794.

Kwon, C., Qian, L., Cheng, P., Nigam, V., Arnold, J., and Srivastava, D. (2009). A regulatory pathway involving Notch1/beta-catenin/Isl1 determines cardiac progenitor cell fate. Nat. Cell Biol. *11*, 951–957.

Lehman, J.J., Barger, P.M., Kovacs, A., Saffitz, J.E., Medeiros, D.M., and Kelly, D.P. (2000). Peroxisome proliferator-activated receptor gamma coactivator-1 promotes cardiac mitochondrial biogenesis. J. Clin. Invest. *106*, 847–856.

Li, X., Martinez-Fernandez, A., Hartjes, K.A., Kocher, J.-P.A., Olson, T.M., Terzic, A., and Nelson, T.J. (2014). Transcriptional atlas of cardiogenesis maps congenital heart disease interactome. Physiol. Genomics *46*, 482–495.

Lopaschuk, G.D., Collins-Nakai, R.L., and Itoi, T. (1992). Developmental changes in energy substrate use by the heart. Cardiovasc. Res. *26*, 1172–1180.

Lundy, S.D., Zhu, W.-Z., Regnier, M., and Laflamme, M.A. (2013). Structural and functional maturation of cardiomyocytes derived from human pluripotent stem cells. Stem Cells Dev. *22*, 1991–2002.

McCall, M.N., Bolstad, B.M., and Irizarry, R.A. (2010). Frozen robust multiarray analysis (fRMA). Biostatistics *11*, 242–253.

McKinney-Freeman, S., Cahan, P., Li, H., Lacadie, S.A., Huang, H.-T., Curran, M., Loewer, S., Naveiras, O., Kathrein, K.L., Konantz, M., et al. (2012). The transcriptional landscape of hematopoietic stem cell ontogeny. Cell Stem Cell *11*, 701–714.

Miller, J.A., Ding, S.-L., Sunkin, S.M., Smith, K.A., Ng, L., Szafer, A., Ebbert, A., Riley, Z.L., Royall, J.J., Aiona, K., et al. (2014). Transcriptional landscape of the prenatal human brain. Nature *508*, 199–206.

Nunes, S.S., Miklas, J.W., Liu, J., Aschar-Sobbi, R., Xiao, Y., Zhang, B., Jiang, J., Massé, S., Gagliardi, M., Hsieh, A., et al. (2013). Biowire: a platform for maturation of human pluripotent stem cell-derived cardiomyocytes. Nat. Methods *10*, 781–787.

O'Meara, C.C., Wamstad, J.A., Gladstone, R.A., Fomovsky, G.M., Butty, V.L., Shrikumar, A., Gannon, J.B., Boyer, L.A., and Lee, R.T. (2015). Transcriptional reversion of cardiac myocyte fate during mammalian cardiac regeneration. Circ. Res. *116*, 804–815.

Raychaudhuri, S., Stuart, J.M., and Altman, R.B. (2000). Principal components analysis to summarize microarray experiments: application to sporulation time series. Pac. Symp. Biocomput. *2000*, 455–466.

Ringnér, M. (2008). What is principal component analysis? Nat. Biotechnol. *26*, 303–304.

Ritchie, M.E., Phipson, B., Wu, D., Hu, Y., Law, C.W., Shi, W., and Smyth, G.K. (2015). limma powers differential expression analyses for RNA-sequencing and microarray studies. Nucleic Acids Res. *43*, e47.

Salick, M.R., Napiwocki, B.N., Sha, J., Knight, G.T., Chindhy, S.A., Kamp, T.J., Ashton, R.S., and Crone, W.C. (2014). Micropattern width dependent sarcomere development in human ESC-derived cardiomyocytes. Biomaterials *35*, 4454–4464.

Seita, J., Sahoo, D., Rossi, D.J., Bhattacharya, D., Serwold, T., Inlay, M.A., Ehrlich, L.I.R., Fathman, J.W., Dill, D.L., and Weissman, I.L. (2012). Gene Expression Commons: an open platform for absolute gene expression profiling. PLoS ONE *7*, e40321.

Seo, K., Rainer, P.P., Shalkey Hahn, V., Lee, D.-I., Jo, S.-H., Andersen, A., Liu, T., Xu, X., Willette, R.N., Lepore, J.J., et al. (2014). Combined TRPC3 and TRPC6 blockade by selective small-molecule or genetic deletion inhibits pathological cardiac hypertrophy. Proc. Natl. Acad. Sci. USA *111*, 1551–1556.

Shenje, L.T., Andersen, P., Uosaki, H., Fernandez, L., Rainer, P.P., Cho, G.-S., Lee, D.-I., Zhong, W., Harvey, R.P., Kass, D.A., and Kwon, C. (2014). Precardiac deletion of Numb and Numblike reveals renewal of cardiac progenitors. eLife *3*, e02164.

Srivastava, D. (2006). Making or breaking the heart: from lineage determination to morphogenesis. Cell *126*, 1037–1048.

Tseng, A.-S., Engel, F.B., and Keating, M.T. (2006). The GSK-3 inhibitor BIO promotes proliferation in mammalian cardiomyocytes. Chem. Biol. *13*, 957–963.

Uosaki, H., Fukushima, H., Takeuchi, A., Matsuoka, S., Nakatsuji, N., Yamanaka, S., and Yamashita, J.K. (2011). Efficient and scalable purification of cardiomyocytes from human embryonic and induced pluripotent stem cells by VCAM1 surface expression. PLoS ONE *6*, e23657.

Uosaki, H., Andersen, P., Shenje, L.T., Fernandez, L., Christiansen, S.L., and Kwon, C. (2012). Direct contact with endoderm-like cells efficiently induces cardiac progenitors from mouse and human pluripotent stem cells. PLoS ONE *7*, e46413.

Uosaki, H., Magadum, A., Seo, K., Fukushima, H., Takeuchi, A., Nakagawa, Y., Moyes, K.W., Narazaki, G., Kuwahara, K., Laflamme, M., et al. (2013). Identification of chemicals inducing cardiomyocyte proliferation in developmental stage-specific manner with pluripotent stem cells. Circ Cardiovasc Genet *6*, 624–633.

Vreeker, A., van Stuijvenberg, L., Hund, T.J., Mohler, P.J., Nikkels, P.G.J., and van Veen, T.A.B. (2014). Assembly of the cardiac intercalated disk during pre- and postnatal development of the human heart. PLoS ONE *9*, e94722.

Wada, R., Muraoka, N., Inagawa, K., Yamakawa, H., Miyamoto, K., Sadahiro, T., Umei, T., Kaneda, R., Suzuki, T., Kamiya, K., et al. (2013). Induction of human cardiomyocyte-like cells from fibroblasts by defined factors. Proc. Natl. Acad. Sci. USA *110*, 12667–12672.

Yamanaka, S., Zahanich, I., Wersto, R.P., and Boheler, K.R. (2008). Enhanced proliferation of monolayer cultures of embryonic stem (ES) cell-derived cardiomyocytes following acute loss of retinoblastoma. PLoS ONE *3*, e3896.

Yamashita, J., Itoh, H., Hirashima, M., Ogawa, M., Nishikawa, S., Yurugi, T., Naito, M., Nakao, K., and Nishikawa, S. (2000). Flk1-positive cells derived from embryonic stem cells serve as vascular progenitors. Nature *408*, 92–96.

Yanagi, K., Takano, M., Narazaki, G., Uosaki, H., Hoshino, T., Ishii, T., Misaki, T., and Yamashita, J.K. (2007). Hyperpolarization-activated cyclic nucleotide-gated channels and T-type calcium channels confer automaticity of embryonic stem cell-derived cardiomyocytes. Stem Cells *25*, 2712–2719.

Yang, X., Rodriguez, M., Pabon, L., Fischer, K.A., Reinecke, H., Regnier, M., Sniadecki, N.J., Ruohola-Baker, H., and Murry, C.E. (2014). Tri-iodo-l-thyronine promotes the maturation of human cardiomyocytes-derived from induced pluripotent stem cells. J. Mol. Cell. Cardiol. *72*, 296–304.

Ziman, A.P., Gómez-Viquez, N.L., Bloch, R.J., and Lederer, W.J. (2010). Excitation-contraction coupling changes during postnatal cardiac development. J. Mol. Cell. Cardiol. *48*, 379–386.